



You have downloaded a document from  
**RE-BUŚ**  
repository of the University of Silesia in Katowice

**Title:** Thermal stability, crystallization and magnetic properties of Fe-Co-based metallic glasses

**Author:** S. Lesz, Piotr Kwapuliński, M. Nabiałek, P. Zackiewicz, L. Hawelek

**Citation style:** Lesz S., Kwapuliński Piotr, Nabiałek M., Zackiewicz P., Hawelek L. (2016). Thermal stability, crystallization and magnetic properties of Fe-Co-based metallic glasses. "Journal of Thermal Analysis and Calorimetry" (Vol. 125, nr 3 (2016), s. 1143-1149), doi 10.1007/s10973-016-5430-x



Uznanie autorstwa - Licencja ta pozwala na kopiowanie, zmienianie, rozprowadzanie, przedstawianie i wykonywanie utworu jedynie pod warunkiem oznaczenia autorstwa.



# Thermal stability, crystallization and magnetic properties of Fe-Co-based metallic glasses

S. Lesz<sup>1</sup> · P. Kwapuliński<sup>2</sup> · M. Nabilek<sup>3</sup> · P. Zackiewicz<sup>4</sup> · L. Hawelek<sup>4</sup>

Received: 15 October 2015 / Accepted: 28 March 2016 / Published online: 11 April 2016  
© The Author(s) 2016. This article is published with open access at Springerlink.com

**Abstract** The aim of the paper was to investigate thermal stability, crystallization and magnetic properties of Fe-Co-based metallic glasses (MGs). Investigations were carried out on amorphous ribbons with the compositions of  $[(\text{Fe}_{0.5}\text{Co}_{0.5})_{0.75}\text{B}_{0.2}\text{Si}_{0.05}]_{96}\text{Nb}_4$  and  $[(\text{Fe}_{0.6}\text{Co}_{0.3}\text{Ni}_{0.1})_{0.75}\text{B}_{0.2}\text{Si}_{0.05}]_{96}\text{Nb}_4$ . Thermal properties (liquidus  $T_l$  and melting  $T_m$  temperatures) of the pre-alloyed ingots upon heating and cooling were analyzed by DTA at a heating/cooling rate of  $0.33 \text{ K s}^{-1}$  under the purified argon atmosphere. The structure of the ribbons was examined by X-ray diffraction (XRD) and transmission electron microscopy (TEM) method. Kinetics of the crystallization process was examined by applying differential scanning calorimetry (DSC) method, and experiments performed in thermal analysis involve heating at a constant rates  $\beta = 0.17, 0.33$  and  $0.5 \text{ K s}^{-1}$ . Additionally, the conventional crystallization temperature  $T_x$  was determined from the normalized isochronal resistivity curves  $\alpha(T)$  with heating rate  $0.0083 \text{ K s}^{-1}$ .  $\alpha$  is the temperature coefficient of resistance and  $\alpha = \rho^{-1} d\rho/dT$ . The  $T_x$  can be obtained from the condition  $\alpha = 0$  (Stokłosa et al. in J Alloy Compd 509(37):9050–9054, 2011). The saturation magnetization

$M(T)$  was measured in situ with heating rates  $0.083 \text{ K s}^{-1}$  using magnetic balance (Szewieczek and Lesz in J Mater Process Tech 162–163:254–259, 2005).

**Keywords** Amorphous materials · Crystallization · Thermal stability · Magnetic properties

## Introduction

Multicomponent Fe-Co-based amorphous alloys (metallic glasses) play a central role in technological innovation because of their use in a wide range of applications, i.e., precision mold material, precision imprint material, precision sensor material, precision machinery material, surface coating material, cutting tool material, shot penning material, fuel cell separator material and so forth [1, 3–5].

The Fe-Co-based metallic glasses (MGs) have attracted much attention of the scientists working in the field of materials science due to their promising mechanical and functional properties. The Fe-Co-based MGs have been intensively investigated as soft magnetic materials for high-temperature applications since controlled addition of Co enhances the Curie temperature. The Fe-Co-based MGs exhibit good soft magnetic properties, i.e., high saturation magnetization (0.8–1.3 T) and low coercivity ( $1\text{--}2.5 \text{ A m}^{-1}$ ) [6]. More recently, microalloying has been found to be an effective way to improve the properties of the base MGs [7–10]. For example, Ni has been introduced to some BMGs to enhance their ductility [11], fatigue resistance [12], soft magnetic properties [13] and glass-forming ability (GFA) [14] of the systems. The magnetic properties of MGs are dependent on Ni, Co and Fe contents. The decrease in coercivity ( $H_c$ ) with increasing Co content has been recognized to originate from the reduction of saturation magnetostriction [3].

✉ S. Lesz  
sabina.lesz@polsl.pl

<sup>1</sup> Institute of Engineering Materials and Biomaterials, Silesian University of Technology, 18a Konarskiego Street, 44-100 Gliwice, Poland

<sup>2</sup> Institute of Materials Science, University of Silesia, 1A, 75 Pułku Piechoty Street, Chorzów 41-500, Poland

<sup>3</sup> Institute of Physics, Czestochowa University of Technology, 19 Av. Armii Krajowej, Czestochowa 42-200, Poland

<sup>4</sup> Institute of Non-Ferrous Metals, 5 Sowinskiego Street, 44-100 Gliwice, Poland

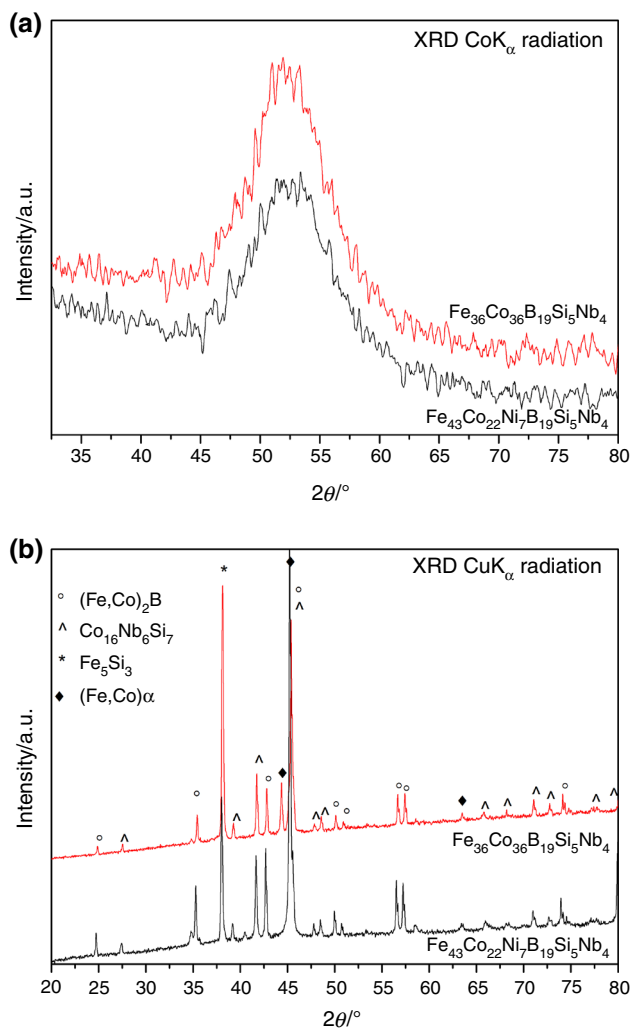


**Fig. 1** X-ray diffraction pattern of the  $\text{Fe}_{36}\text{Co}_{36}\text{B}_{19}\text{Si}_5\text{Nb}_4$  and  $\text{Fe}_{43}\text{Co}_{22}\text{Ni}_7\text{B}_{19}\text{Si}_5\text{Nb}_4$  alloys in the as quenched state (a) and after annealing at 1000 K (b)

The addition of small amounts of Nb to (Fe,Co,Ni)-(B,Si) alloys is effective for the increase in GFA through the increase in the stability of supercooled liquid (SL) against crystallization [6]. The addition of 4 at.% Nb was found to be very effective in improving the GFA of Fe- and Co-based glassy alloys [15].

Metalloid elements of Si and B play crucial role in the formation of the BMGs and have effect on the GFA, thermal stability, crystallization and properties of the BMGs. These materials have a strong affinity with conventional BMGs base elements such Fe and rare earth elements, i.e., they have large negative heat of mixing with these base elements. The metalloid elements would result in crystallization and degrade the GFA of the BMGs, but on the other hand, due to the small atomic size of Si and B atoms, the proper addition can tighten the alloy structure and then stabilize the alloy against crystallization [6].

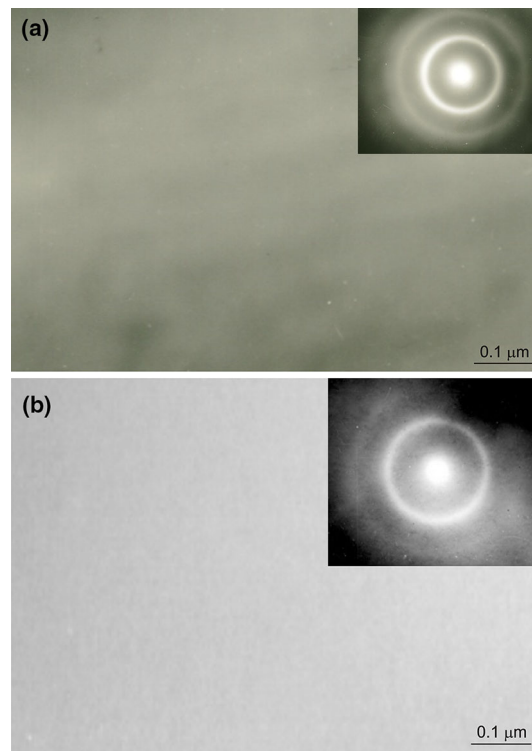


**Fig. 2** TEM micrograph and selected area electron diffraction pattern of  $\text{Fe}_{36}\text{Co}_{36}\text{B}_{19}\text{Si}_5\text{Nb}_4$  (a) and  $\text{Fe}_{43}\text{Co}_{22}\text{Ni}_7\text{B}_{19}\text{Si}_5\text{Nb}_4$  (b) alloys in the as quenched state

It is natural and interesting to examine the effects of replacing part of Fe by other magnetic elements, Co and Ni, thermal, magnetic and electrical properties of the Fe-Co-based metallic glasses. In this paper, effect of Ni addition on structure and kinetics of the crystallization process of Fe-Co-based metallic glasses (MGs) prepared from industrial raw materials are reported.

## Experimental

Investigations were carried out on amorphous ribbons with compositions of  $[(\text{Fe}_{0.5}\text{Co}_{0.5})_{0.75}\text{B}_{0.2}\text{Si}_{0.05}]_{96}\text{Nb}_4$  and  $[(\text{Fe}_{0.6}\text{Co}_{0.3}\text{Ni}_{0.1})_{0.75}\text{B}_{0.2}\text{Si}_{0.05}]_{96}\text{Nb}_4$ . The Fe-based master alloy ingots were prepared by melting the mixtures of the Fe-B (Fe 85.4 B 14.5 mass%), Fe-Nb (Fe 31.4 Nb 68.5 mass%), Fe-Si (Fe 42.7 Si 57.2 mass%) starting ferroalloys and pure Fe (99.99 mass %), Co (99.99 mass %), Ni (99.99 mass%), metals in an argon atmosphere. The content of boron in the cast alloy was adjusted by adding the Fe-B alloy, which is much cheaper than pure boron. The  $\text{Fe}_{36}\text{Co}_{36}\text{B}_{19}\text{Si}_5\text{Nb}_4$  and  $\text{Fe}_{43}\text{Co}_{22}\text{Ni}_7\text{B}_{19}\text{Si}_5\text{Nb}_4$  alloy compositions represent nominal atomic percentages. Ribbons with thickness of 0.07 mm and width of 2.3 mm were prepared by the single copper roller melt spinning method.

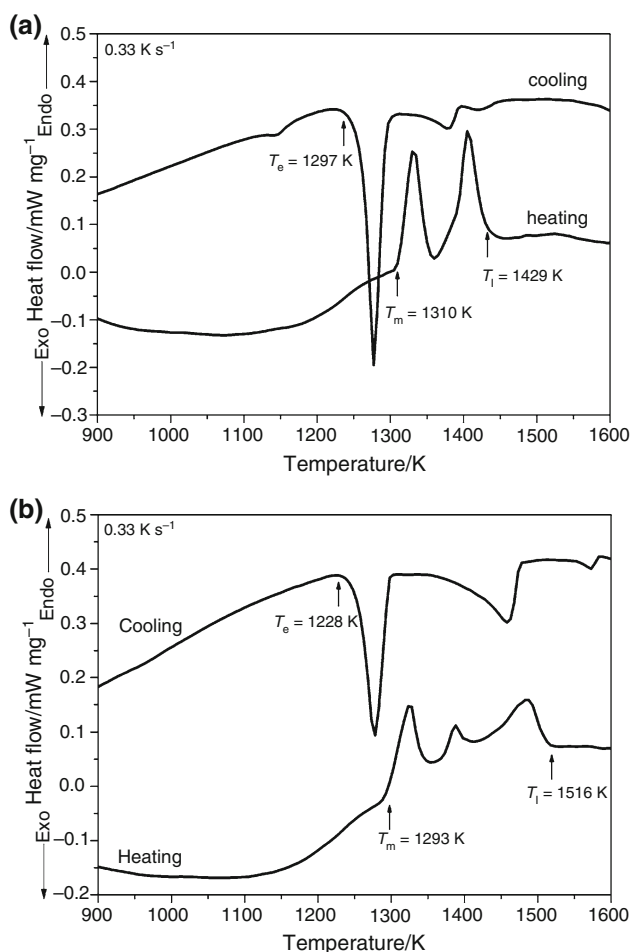


**Fig. 3** Differential thermal analysis (DTA) curves of the pre-alloyed ingots of the  $\text{Fe}_{36}\text{Co}_{36}\text{B}_{19}\text{Si}_5\text{Nb}_4$  (a) and  $\text{Fe}_{43}\text{Co}_{22}\text{Ni}_7\text{B}_{19}\text{Si}_5\text{Nb}_4$  alloy (b) under the heating/cooling rate of  $0.33 \text{ K s}^{-1}$

The master alloy was melted in a quartz crucible using an induction coil and pushed thereafter on a copper wheel by applying an ejection pressure of about 0.02 MPa.

The structure of the as quenched ribbons was identified by X-ray diffraction (XRD) method on a X-Pert PRO MP diffractometer using filtered  $\text{Co-K}\alpha$  radiation ( $\lambda = 0.17888 \text{ nm}$ ), a tube voltage of 30 kV and a current of 10 mA, in Bragg–Brentano geometry. For the ribbons after annealing at 1000 K, XRD measurements were performed at ambient temperature using a Rigaku MiniFlex 600 diffractometer (Rigaku Corporation, Tokyo, Japan) with  $\text{Cu K}\alpha$  radiation ( $\lambda = 0.15406 \text{ nm}$ ), a tube voltage of 40 kV and a current of 15 mA using a D/teX Ultra silicon strip detector. In order to conduct structural study, the transmission electron microscope (TEM) TESLA BS 540 was used.

Thermal properties liquidus  $T_l$  and melting temperatures  $T_m$  of the pre-alloyed ingots (as well as the base alloy and the alloy with 7.0 at.% nickel addition) upon heating and

cooling were analyzed by DTA at a heating/cooling rate of  $0.33 \text{ K s}^{-1}$  under the purified argon atmosphere. The DTA measurements were carried out with a NETZSCH model DSC 404 C Pegasus.

Crystallization process was examined by applying isochronal DSC (NETZSCH STA 449F3) method with heating rate  $\beta = 0.17, 0.33$  and  $0.5 \text{ K s}^{-1}$ . Activation energies of crystallization process were obtained by applying the Kissinger method. Additionally, the relative crystallization temperature  $T_x$  was determined from the normalized isochronal resistivity curves  $\alpha(T)$  ( $0.0083 \text{ K s}^{-1}$ );  $\alpha$  is the temperature coefficient of resistance and  $\alpha = \rho^{-1} d\rho/dT$ . The  $T_x$ , can be obtained from the condition  $\alpha = 0$  [1, 16].

The saturation magnetization  $M(T)$  was measured in situ with heating rates  $0.083 \text{ K s}^{-1}$  using magnetic balance. The family of magnetization curves  $M_{\text{norm}}(T)$  normalized to the value at 300 K, and the corresponding  $dM/dT$  curves were presented. The Curie temperature  $T_C$  is determined from the condition  $dM/dT = \text{minimum}$  [2].

For samples in the as quenched state, the relative magnetic permeability (Maxwell–Wien bridge, frequency 1 kHz, magnetic field  $0.5 \text{ A m}^{-1}$ ) at room temperature was obtained.

The measurements of magnetic permeability  $\mu_i$  (at force  $H \approx 0.5 \text{ A m}^{-1}$  and frequency  $f \approx 1 \text{ kHz}$ ) and the intensity of magnetic after effect  $\Delta\mu/\mu(t_1)$  ( $\Delta\mu = \mu(t_1 = 30 \text{ s}) - \mu(t_2 = 1800 \text{ s})$ ), where  $\mu$  is the initial magnetic permeability measured at time  $t$  after demagnetization, have been done. The investigations of ribbons in as quenched state were performed with the use of automatic device for measurements magnetic permeability [1].

## Results and discussion

It was found from the obtained results of structural studies performed by X-ray diffraction and that diffraction pattern of ribbons of the  $\text{Fe}_{36}\text{Co}_{36}\text{B}_{19}\text{Si}_5\text{Nb}_4$  and  $\text{Fe}_{43}\text{Co}_{22}\text{Ni}_7\text{B}_{19}\text{Si}_5\text{Nb}_4$  alloy consists of a broad-angle peak (Fig. 1a). The typical diffused scattering indicates the presence of the amorphous structure with no crystalline peaks. Obtained results of structural studies performed by X-ray diffraction are corresponding with the HRTEM micrograph. The diffraction pattern taken from the small region consists only of halo rings, and no appreciable reflection spots of crystalline phases are seen (Fig. 2a, b). After annealing at 1000 K, few crystalline phases fully indexed both diffraction patterns and they are  $(\text{Fe,Co})_2\text{B}$ ,  $\text{Co}_{16}\text{Nb}_6\text{Si}_7$ ,  $\text{Fe}_5\text{Si}_3$  and  $(\text{Fe,Co})\alpha$  (Fig. 1b).

The thermal properties of the pre-alloyed ingots  $\text{Fe}_{36}\text{Co}_{36}\text{B}_{19}\text{Si}_5\text{Nb}_4$  and  $\text{Fe}_{43}\text{Co}_{22}\text{Ni}_7\text{B}_{19}\text{Si}_5\text{Nb}_4$  alloy upon heating measured by DTA are presented on Fig. 3a, b. The  $\text{Fe}_{36}\text{Co}_{36}\text{B}_{19}\text{Si}_5\text{Nb}_4$  alloy presents clearly two endothermic

**Fig. 4** Temperature coefficient of resistance  $\alpha$  versus temperature of  $\text{Fe}_{36}\text{Co}_{36}\text{B}_{19}\text{Si}_5\text{Nb}_4$  (a) and  $\text{Fe}_{43}\text{Co}_{22}\text{Ni}_7\text{B}_{19}\text{Si}_5\text{Nb}_4$  (b) ribbons obtained on the basis of measurements of electric resistivity  $\rho$  as function of temperature  $T$  with heating rate  $0.0083 \text{ K s}^{-1}$

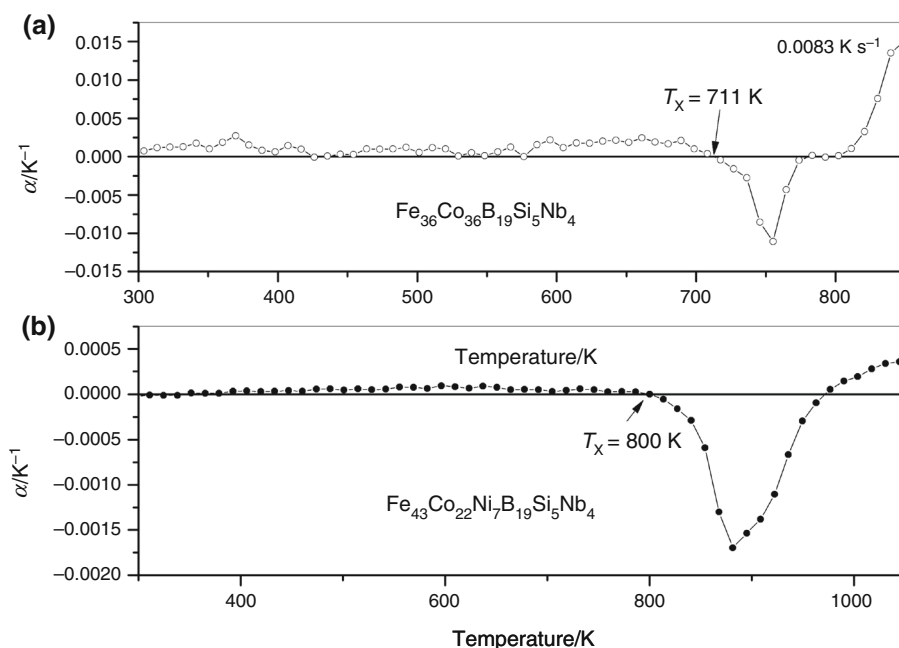
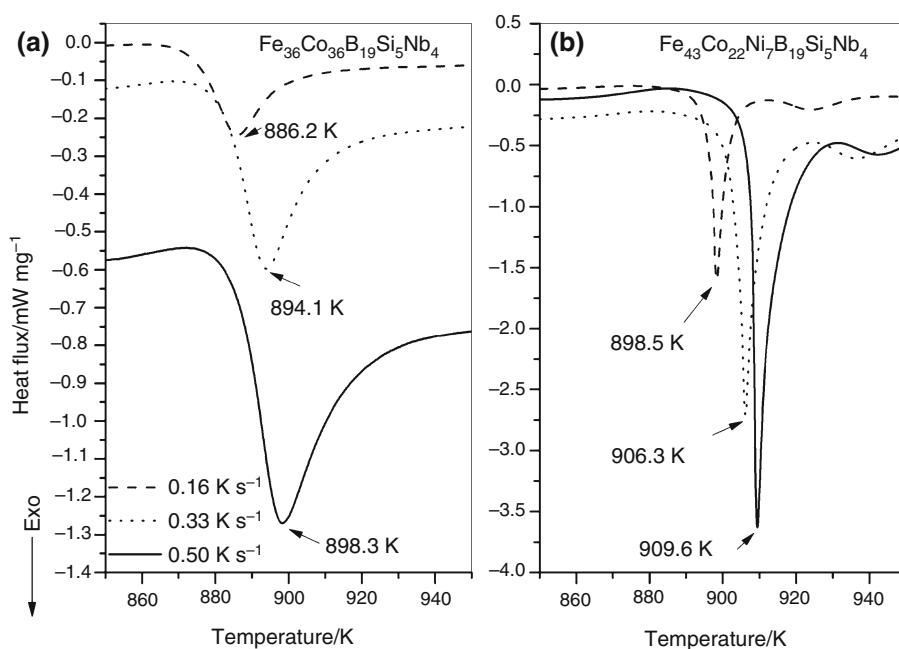


**Fig. 5** The DSC measurements with different linear heating rates (0.16, 0.33,  $0.50 \text{ K s}^{-1}$ ) for  $\text{Fe}_{36}\text{Co}_{36}\text{B}_{19}\text{Si}_5\text{Nb}_4$  (a) and  $\text{Fe}_{43}\text{Co}_{22}\text{Ni}_7\text{B}_{19}\text{Si}_5\text{Nb}_4$  (b) alloys



peaks (Fig. 3a), but  $\text{Fe}_{43}\text{Co}_{22}\text{Ni}_7\text{B}_{19}\text{Si}_5\text{Nb}_4$  alloy presents three endothermic peaks. The first peak for  $\text{Fe}_{36}\text{Co}_{36}\text{B}_{19}\text{Si}_5\text{Nb}_4$  and  $\text{Fe}_{43}\text{Co}_{22}\text{Ni}_7\text{B}_{19}\text{Si}_5\text{Nb}_4$  alloy begins near the melting point  $T_m$  and onset is 1310 and 1293 K, respectively. The maximum signal of the second peak is separate for the  $\text{Fe}_{36}\text{Co}_{36}\text{B}_{19}\text{Si}_5\text{Nb}_4$  alloys. This signal is associated with the liquidus temperature  $T_l$  [17, 18]. As shown in Fig. 3a, b, with the replacing part of Co by Ni in the Fe-Co-based metallic glasses,  $T_l$  increases from 1429 to 1516 K.

Figure 3a, b shows thermal properties of the pre-alloyed ingots  $\text{Fe}_{36}\text{Co}_{36}\text{B}_{19}\text{Si}_5\text{Nb}_4$  and  $\text{Fe}_{43}\text{Co}_{22}\text{Ni}_7\text{B}_{19}\text{Si}_5\text{Nb}_4$  alloys upon cooling measured by DTA. For the  $\text{Fe}_{36}\text{Co}_{36}\text{B}_{19}\text{Si}_5\text{Nb}_4$  alloy, two peaks are clearly shown (Fig. 3a). The first peak corresponds to the eutectic temperature  $T_e$ —1297 K. The eutectic temperature,  $T_e$ , decreases with Ni addition.

Figure 4 shows the temperature coefficient of resistance  $\alpha = \rho^{-1} d\rho/dT$  versus temperature  $T$  for the  $\text{Fe}_{36}\text{Co}_{36}\text{B}_{19}\text{Si}_5\text{Nb}_4$  and  $\text{Fe}_{43}\text{Co}_{22}\text{Ni}_7\text{B}_{19}\text{Si}_5\text{Nb}_4$  alloys. Initially,  $\rho$

**Fig. 6** The Kissinger plot for  $\text{Fe}_{36}\text{Co}_{36}\text{B}_{19}\text{Si}_5\text{Nb}_4$  (a) and  $\text{Fe}_{43}\text{Co}_{22}\text{Ni}_7\text{B}_{19}\text{Si}_5\text{Nb}_4$  (b) alloys

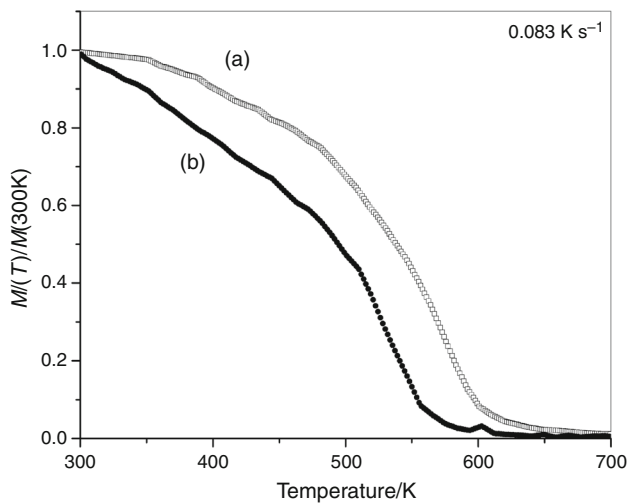
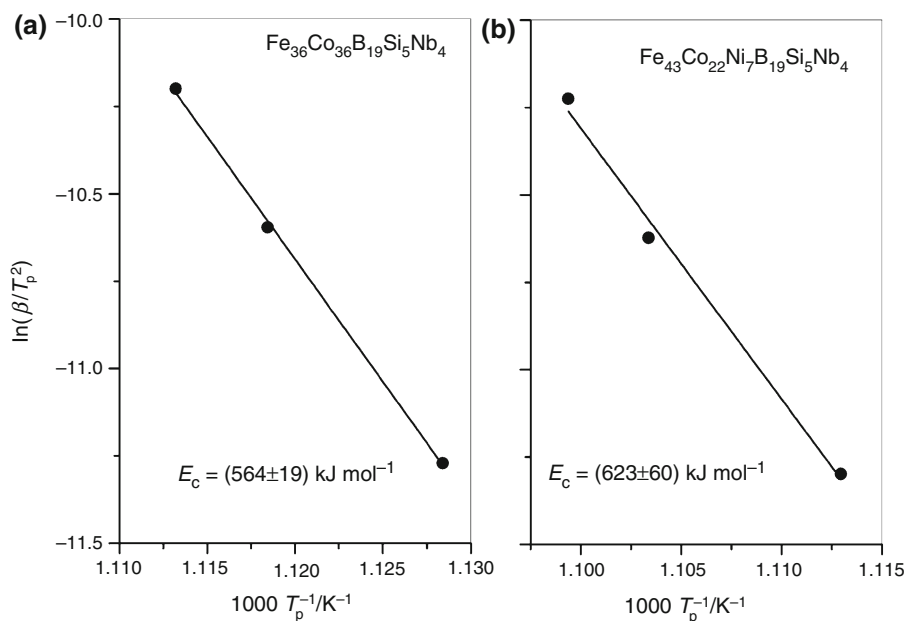


**Fig. 7** Normalized magnetization  $M_{\text{norm}}$  versus temperature  $T$  of  $\text{Fe}_{36}\text{Co}_{36}\text{B}_{19}\text{Si}_5\text{Nb}_4$  (a) and  $\text{Fe}_{43}\text{Co}_{22}\text{Ni}_7\text{B}_{19}\text{Si}_5\text{Nb}_4$  (b) ribbons obtained with heating rate  $0.083 \text{ K s}^{-1}$

increases ( $\alpha \sim \text{const}$ ) with increasing temperature due to electron–phonon scattering in amorphous structure.

At higher temperatures, an abrupt drop of resistivity is observed ( $\alpha$ -negative) which is surely related to first stage of crystallization. An arbitrary taken condition  $\alpha = 0$  allows defining the so-called crystallization temperature  $T_x$ , which depends on heating rate, as it should be expected for any diffusion-controlled process. Basing on curves  $\alpha(T)$  determined on the basis of measurements of electric resistivity  $\rho$  as function of temperature  $T$ , it was found that crystallization temperatures  $T_x$  of  $\text{Fe}_{36}\text{Co}_{36}\text{B}_{19}\text{Si}_5\text{Nb}_4$  and  $\text{Fe}_{43}\text{Co}_{22}\text{Ni}_7\text{B}_{19}\text{Si}_5\text{Nb}_4$  ribbons are equal  $T_x = 711 \text{ K}$  and

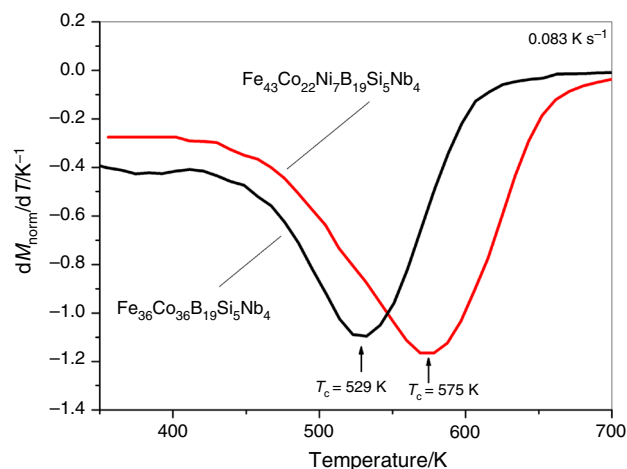


**Fig. 8**  $dM_{\text{norm}}(T)/dT$  curves for the data presented in Fig. 7

$800 \text{ K}$ , respectively (Fig. 4). The crystallization of metallic glasses is a kinetics transition. Leaving the metallic glasses at a temperature that is close to  $T_x$  may crystallize the amorphous structures, which often degrades the excellent mechanical and magnetic performance of metallic glasses. In addition,  $T_x$  also sets the upper temperature limit of magnetic annealing, which is often used to modify or improve the magnetic properties. Therefore, increase  $T_x$  from 711 to 800 K with Ni addition is very advantageous.

Crystallization process was examined by applying DSC measurements with different linear heating rates ( $0.16, 0.33, 0.5 \text{ K s}^{-1}$ ). Based on this kind of measurement, activation energies of crystallization were calculated using the Kissinger method [19]. Figure 5 shows DSC curves

**Table 1** Thermal stability ( $T_C$  Curie temperature,  $T_x$  crystallization temperature) and magnetic properties ( $H_c$  coercivity,  $\mu_i$  initial magnetic permeability,  $\Delta\mu \mu^{-1}$  magnetic after effects) of  $\text{Fe}_{36}\text{Co}_{36}\text{B}_{19}\text{Si}_5\text{Nb}_4$  and  $\text{Fe}_{43}\text{Co}_{22}\text{Ni}_7\text{B}_{19}\text{Si}_5\text{Nb}_4$  ribbons

Alloy	$\mu_i$	$\Delta\mu \mu^{-1}/\%$	$H_c/\text{A m}^{-1}$	$T_c/\text{K}$	$T_m/\text{K}$	$T_C/\text{K}$	$T_x/\text{K}$	$T_f/\text{K}$
$\text{Fe}_{36}\text{Co}_{36}\text{B}_{19}\text{Si}_5\text{Nb}_4$	3000	5.0	4.0	1297	1310	575	711	1429
$\text{Fe}_{43}\text{Co}_{22}\text{Ni}_7\text{B}_{19}\text{Si}_5\text{Nb}_4$	1600	4.5	4.0	1228	1293	529	800	1516

obtained for different heating rates  $\beta$ . With increasing  $\beta$ , the observed DSC minimum shifts into higher temperatures. As the crystallization process is a diffusion-controlled phenomenon, its evolution with time can be described by the kinetic rate equation with the effective overall reaction rate obeying an Arrhenius relation. The activation energy  $E$  describing the crystallization process should fulfill the Kissinger equation:

$$\ln \frac{\beta}{T_p^2} = -\frac{E_c}{RT_p} + \ln \frac{K_0 E_c}{R} \quad (1)$$

where  $T_p$  is the characteristic temperature (position of the DSC peak) determined for the heating rate  $\beta$ ,  $R$  is the gas constant, and  $K_0$  is the Arrhenius equation pre-exponential factor. According to Eq. (1), a plot of  $\ln(\beta/T_p^2)$  versus  $1/T_p$  should yield a straight line with the slope  $E_c/R$ .

Figure 5 shows the family of DSC curves obtained for the  $\text{Fe}_{36}\text{Co}_{36}\text{B}_{19}\text{Si}_5\text{Nb}_4$  (a) and  $\text{Fe}_{43}\text{Co}_{22}\text{Ni}_7\text{B}_{19}\text{Si}_5\text{Nb}_4$  (b) alloys (heating rate 0.16, 0.33, 0.50  $\text{K s}^{-1}$ ). For different heating rates, a shift in temperature of the homologous points of DSC curves was observed. Using these data and the Kissinger method, activation energies of the crystallization were determined (Fig. 6). For the  $\text{Fe}_{36}\text{Co}_{36}\text{B}_{19}\text{Si}_5\text{Nb}_4$  and  $\text{Fe}_{43}\text{Co}_{22}\text{Ni}_7\text{B}_{19}\text{Si}_5\text{Nb}_4$  alloys, we have obtained,  $E_c = 564$  and  $E_c = 623 \text{ kJ mol}^{-1}$ , respectively. The activation energy is quite high, more than double than the energies measured for the good glass formers in Zr-based alloy [20] and close to those of measured for the  $[(\text{Fe}_{0.5}\text{Co}_{0.5})_{0.75}\text{B}_{0.20}\text{Si}_{0.05}]_{96}\text{Nb}_4$  alloy [21, 22].

Figure 7 shows the normalized magnetization in saturation  $M_{\text{norm}} = M(T)/M(300 \text{ K})$  versus temperature measured at magnetic field 0.5 T and heating rate 0.083  $\text{K s}^{-1}$  for the  $\text{Fe}_{36}\text{Co}_{36}\text{B}_{19}\text{Si}_5\text{Nb}_4$  and  $\text{Fe}_{43}\text{Co}_{22}\text{Ni}_7\text{B}_{19}\text{Si}_5\text{Nb}_4$  alloys. In the temperature range  $300 \text{ K} < T < 575 \text{ K}$ , magnetization monotonically decreases up to the Curie temperature of amorphous phase.

The values of  $T_C$ , for examined alloys, were determined from the inflection point of  $M(T)$  curve which is a commonly used procedure (Fig. 8). The value of Curie temperature for the  $\text{Fe}_{36}\text{Co}_{36}\text{B}_{19}\text{Si}_5\text{Nb}_4$  and  $\text{Fe}_{43}\text{Co}_{22}\text{Ni}_7\text{B}_{19}\text{Si}_5\text{Nb}_4$  ribbons of thickness of 0.07 mm is equal 575 and 529 K, respectively (Figs. 7a, b, 8a, b). The similar value of  $T_C$  was obtained in [23].

The results of magnetic properties measurements of the investigated ribbons of the  $\text{Fe}_{36}\text{Co}_{36}\text{B}_{19}\text{Si}_5\text{Nb}_4$  and

$\text{Fe}_{43}\text{Co}_{22}\text{Ni}_7\text{B}_{19}\text{Si}_5\text{Nb}_4$  alloys have been presented in the Table 1. The ribbons of  $\text{Fe}_{36}\text{Co}_{36}\text{B}_{19}\text{Si}_5\text{Nb}_4$  alloy have magnetic properties ( $H_c = 4.0 \text{ A m}^{-1}$ ,  $\mu_i = 3000$ ,  $\Delta\mu \mu^{-1} = 5.0$ , Table 1) similar than for ribbons of  $\text{Fe}_{43}\text{Co}_{22}\text{Ni}_7\text{B}_{19}\text{Si}_5\text{Nb}_4$  alloy ( $H_c = 4.0 \text{ A m}^{-1}$ ,  $\mu_i = 1600$ ,  $\Delta\mu \mu^{-1} = 4.5$ , Table 1). The value of  $H_c$  and  $T_C$  obtained for the ribbons of  $\text{Fe}_{36}\text{Co}_{36}\text{B}_{19}\text{Si}_5\text{Nb}_4$  alloy is similar than for these alloy in rod form with 5 mm diameter investigated by Shen and Inoue [24] whose results as follows:  $H_c = 1.5 \text{ A m}^{-1}$  and  $T_C = 692 \text{ K}$ .

The obtained values of  $H_c$  and  $T_C$  of the ribbons with thickness of 0.07 mm of  $\text{Fe}_{43}\text{Co}_{22}\text{Ni}_7\text{B}_{19}\text{Si}_5\text{Nb}_4$  alloy are similar than in other alloys with the similar chemical composition investigated by Shen et al. [5] whose results for  $[(\text{Fe}_{0.6}\text{Co}_{0.3}\text{Ni}_{0.1})_{0.75}\text{B}_{0.2}\text{Si}_{0.05}]_{96}\text{Nb}_4$  and  $[(\text{Fe}_{0.6}\text{Co}_{0.1}\text{Ni}_{0.3})_{0.75}\text{B}_{0.2}\text{Si}_{0.05}]_{96}\text{Nb}_4$  alloys as follows:  $H_c = 2$ ,  $T_C = 643$  and  $H_c = 2.5 \text{ A m}^{-1}$ ,  $T_C = 554 \text{ K}$ , respectively.

The detailed analysis of data of magnetic properties, i.e.,  $\mu_i$  and  $H_c$  allows to classify the investigated alloys in as quenched state as a soft magnetic material (Table 1). These excellent magnetic properties and high value of temperature of crystallization ( $T_x = 711$  and  $800 \text{ K}$ —Figs. 4, 5; Table 1) lead us to expect that the Fe-Co-based amorphous alloy could be used as a new engineering and functional material intended for parts of inductive components. The microvoids content is often examined using magnetic after effects ( $\Delta\mu \mu^{-1}$ ) measurements. The value of  $\Delta\mu \mu^{-1}$  increases with increasing of microvoids into materials [25].

## Conclusions

We can state that the structure of ribbons as well as  $\text{Fe}_{36}\text{Co}_{36}\text{B}_{19}\text{Si}_5\text{Nb}_4$  and  $\text{Fe}_{43}\text{Co}_{22}\text{Ni}_7\text{B}_{19}\text{Si}_5\text{Nb}_4$  alloy at as quenched state is amorphous.

The addition of Ni to the Fe-Co-based MGs induced a change of thermal and magnetic properties. In the Fe-Co-based MGs for alloy containing Ni in comparison with  $\text{Fe}_{36}\text{Co}_{36}\text{B}_{19}\text{Si}_5\text{Nb}_4$  alloy: (1) The  $T_x$  and  $T_f$  both increase from 711 to 800 K and 1429 to 1516 K, respectively, (2) activation energies of the crystallization increase from 564 to 623  $\text{kJ mol}^{-1}$  (increase in thermal stability MGs), (3) the  $T_C$  decreases from 575 to 529 K, (4) initial magnetic permeability decrease from 3000 to 1600 and (5) magnetic after effects ( $\Delta\mu/\mu$ ) decrease from 5.0 to 4.5 % (increase in time stability).

The investigated alloys have good soft magnetic properties in the as quenched state. After crystallization, soft magnetic properties decrease due to formation of borides. These excellent magnetic properties lead us to expect that the investigated MGs is promising for the future applications as new engineering and functional material on the parts of micromotors and other applications. The results obtained for the melt-spun glassy alloy ribbons are the beans for continuation of research on different forms of the investigated alloy, e.g., rods or tubes.

**Acknowledgements** This work was financially supported with statutory funds of Faculty of Mechanical Engineering of Silesian University of Technology in 2015.

**Open Access** This article is distributed under the terms of the Creative Commons Attribution 4.0 International License (<http://creativecommons.org/licenses/by/4.0/>), which permits unrestricted use, distribution, and reproduction in any medium, provided you give appropriate credit to the original author(s) and the source, provide a link to the Creative Commons license, and indicate if changes were made.

## References

- Stokłosa Z, Rasek J, Kwapuliński P, Badura G, Haneczok G, Pająk L, Lelątko J, Kolano-Burian A. Magnetic, electrical and plastic properties of  $\text{Fe}_{76}\text{Nb}_2\text{Si}_{13}\text{B}_9$ ,  $\text{Fe}_{75}\text{Ag}_1\text{Nb}_2\text{Si}_{13}\text{B}_9$  and  $\text{Fe}_{75}\text{Cu}_1\text{Nb}_2\text{Si}_{13}\text{B}_9$  amorphous alloys. *J Alloy Compd.* 2011; 509(37):9050–4.
- Szewieczek D, Lesz S. Influence of structure on the evolution of magnetic and mechanical properties of amorphous and nanocrystalline  $\text{Fe}_{85.4}\text{Hf}_{1.4}\text{B}_{13.2}$  alloy. *J Mater Process Tech.* 2005;162–163:254–9.
- Dobrzański LA, Szindler M, Drygała A, Szindler MM. Silicon solar cells with  $\text{Al}_2\text{O}_3$  antireflection coating. *Cent E J Phys.* 2014;12(9):666–70.
- Dobrzański LA, Tański T, Dobrzańska-Danikiewicz A, Jonda E, Bonek M, Drygała A. Structures, properties and development trends of laser-surface-treated hot-work steels, light metal alloys and polycrystalline silicon, *Laser surface engineering. Processes and applications*, Woodhead Publishing Series in Electronic and Optical Materials 2015;65:3–32.
- Shen B, Chang C, Inoue A. Formation, ductile deformation behaviour and soft-magnetic properties of (Fe Co, Ni)-B-Si-Nb bulk glassy alloys. *Intermetallics.* 2007;15:9–16.
- Wang WH. Roles of minor additions in formation and properties of bulk metallic glasses. *Prog Mater Sci.* 2007;52:540–96.
- Lu ZP, Liu CT, Porter WD. Role of yttrium in glass formation of Fe-based bulk metallic glasses. *Appl Phys Lett.* 2003;83(13): 2581–3.
- Xiao XS, Fang SS, Wang GM, Qin H, Dong YD. Influence of beryllium on thermal stability and glass-forming ability of Zr–Al–Ni–Cu bulk amorphous alloy. *J Alloys Compd.* 2004;376: 145–8.
- Kong KZ, Li Y, Ding J. Effect of boron addition to the hard magnetic bulk  $\text{Nd}_{60}\text{Fe}_{30}\text{Al}_{10}$  amorphous alloy. *J Magn Magn Mater.* 2000;217:65–73.
- Liu L, Qiu CL, Zou H, Chan KC. The effect of the microalloying of Hf on the corrosion behavior of ZrCuNiAl bulk metallic glass. *J Alloys Compd.* 2005;399:144–8.
- Yokoyama Y, Kobayashi A, Fukaura K, Inoue A. Oxygen embrittlement and effect of the addition of Ni element in a bulk amorphous Zr-Cu-Al alloy. *Mater Trans.* 2002;43:571–4.
- Yokoyama Y, Fukaura K, Inoue A. Effect of Ni addition on fatigue properties of bulk glassy  $\text{Zr}_{50}\text{Cu}_{40}\text{Al}_{10}$  alloys. *Mater Trans.* 2004;45:1672–8.
- Wang WH, Pang MX, Zhao DQ, Hu Y, Bai HY. Enhancement of the soft magnetic properties of FeCoZrMoWB bulk metallic glass by microalloying. *J Phys Condens Mat.* 2004;16:3719–23.
- Park ES, Kim WT, Kim DH. The effect of in addition on the glass-forming ability in Cu-Ti-Zr-Ni-Si metallic glasses. *Mater Trans.* 2004;45:2693–6.
- Chang Ch, Shen B, Inoue A. FeNi-based bulk glassy alloys with superhigh mechanical strength and excellent soft magnetic properties. *Appl Phys Lett.* 2006;89:051912.
- Lesz S, Szewczyk R, Szewieczek D, Bieńkowski A. The structure and magnetoelastic properties of the Fe-based amorphous alloy with Hf addition. *J Mater Process Tech.* 2004;157–158:743–8.
- Boettinger WJ, Kattner UR, Moon KW, Perepezko JH. DTA and heat flux DSC measurements of alloy melting and freezing. National Institute of Standards and Technology Special Publication 2006;960–15.
- Lesz S, Babilas R, Nowosielski R. Influence of copper addition on glass forming ability, thermal stability, structure and magnetic properties of Fe-Co-based BMGs. *Solid State Phenom.* 2013; 203–204:296–301.
- Liu F, Liu XN, Wang OJ. Examination of Kissinger's equation for solid-state transformation. *J Alloys Compd.* 2009;473:152–6.
- Prajapati SR, Kasyap S, Patel AT, Pratap A. Non-isothermal crystallization kinetics of  $\text{Zr}_{52}\text{Cu}_{18}\text{Ni}_{14}\text{Al}_{10}\text{Ti}_6$  metallic glass. *J Therm Anal Calorim.* 2015;8:1–13.
- Stoica M, Li R, Yavari AR, Vaughan G, Eckert J, Steenberge N, Romera DR. Thermal stability and magnetic properties of FeCoBSiNb bulk metallic glasses. *J Alloys Compd.* 2010; 504S:123–8.
- Jung HY, Stoica M, Seonghoon Y, Kim DH, Eckert J. Crystallization kinetics of  $\text{Fe}_{76.5-x}\text{C}_{6.0}\text{Si}_{3.3}\text{B}_{5.5}\text{P}_{8.7}\text{Cu}_x$  ( $x = 0, 0.5, \text{ and } 1$  at. pct) bulk amorphous alloy. *Metall Mater Trans A.* 2014;46: 2415–21.
- Nowosielski R, Babilas R. Structure and magnetic properties of  $\text{Fe}_{36}\text{Co}_{36}\text{B}_{19}\text{Si}_5\text{Nb}_4$  bulk metallic glasses. *J Achiev Mater Man Eng.* 2008;30(2):135–40.
- Shen B, Inoue A. Superhigh strength and good soft-magnetic properties of (Fe, Co)-B-Si-Nb bulk glassy alloys with high glass-forming ability. *Appl Phys Lett.* 2004;85(21):4911–3.
- Kronmüller H. Theory of magnetic after-effects in ferromagnetic amorphous alloys. *Philos Mag B.* 1983;48(2):127–50.